

## The Wave–Zonal Mean Flow Interaction in the Southern Hemisphere

HYUN-KYUNG KIM\* AND SUKYOUNG LEE

*Department of Meteorology, The Pennsylvania State University, University Park, Pennsylvania*

(Manuscript received 8 March 2002, in final form 12 November 2003)

### ABSTRACT

This study examines the wave–zonal mean flow interaction in the Southern Hemisphere (SH) and in an SH-like model atmosphere. During the SH winter, when there exist both subtropical and polar front jets, growing baroclinic waves are found between the two jets as well as along the polar front jet. These baroclinic waves between the two jets pump westerly momentum into the interjet region flanked by the subtropical and polar front jets. As a result, these baroclinic waves blend the two jets, preventing the longtime occurrence or establishment of two well-defined jets. It is also shown that during the SH winter, the deceleration of the westerlies on the equatorward side of the subtropical jet is mostly associated with the above baroclinic waves in the interjet region, rather than with eddies that originate along the polar front jet.

A set of idealized numerical model experiments shows that as the value of the surface friction is increased, the direction of the baroclinic wave momentum flux in the interjet region changes, resulting in a drastically different climatological flow.

### 1. Introduction

The current understanding of the role of baroclinic waves for shaping the structure of the zonal mean zonal winds dates back to Starr (1953). However, a more comprehensive picture of the interaction between baroclinic waves and the zonal mean flow was established through both theories (Eliassen and Palm 1961; Andrews and McIntyre 1976, 1978) and explicit numerical calculations of nonlinear baroclinic wave evolutions and diagnostic analysis of observations (e.g., Simmons and Hoskins 1978, 1980; Edmon et al. 1980; Hoskins 1983; Feldstein and Held 1989). These studies, which considered an initial flow consisting of a single jet where the latitude of the maximum baroclinicity coincides with that of the jet, led to the conceptual picture of Held and Hoskins (1985; see their Fig. 3). Initially, wave activity is generated in midlatitudes by baroclinic instability, where the baroclinicity is greatest. The wave activity propagates upward and then equatorward. The net effect

of this wave activity on the zonal mean flow is acceleration at all levels at the source latitudes and deceleration at all levels both equatorward and poleward of the source region. Thus, according to this picture, the maximum poleward eddy heat flux, eddy momentum flux convergence [hence the Eliassen–Palm (EP) flux divergence], and the jet are all latitudinally collocated.

While the above picture has been extremely useful for understanding the impact of the eddies on a zonal mean flow when there is a single midlatitude jet present, such as the Southern Hemisphere summer flow (see Fig. 1a), this picture may not be sufficient when both the subtropical and polar front jets coexist, such as during the winter season. To lowest order, the subtropical jet can be understood as being driven by angular momentum transport associated with the Hadley circulation (Palmén and Newton 1969; Schneider 1977; Held and Hou 1980). The polar front jet (also referred to as the eddy-driven jet), on the other hand, is driven by eddy fluxes associated with Rossby waves (Kuo 1953; Starr 1953; Palmén and Newton; Holopainen 1978; Thompson 1980; Lee and Kim 2003). These waves are generated within the baroclinic zone. Considering these different driving mechanisms, one may expect to find two separate jets, the subtropical jet in lower latitudes and a polar front jet in higher latitudes (Palmén and Newton 1969; Lee and Kim 2003).

For the Southern Hemisphere (SH) winter flow (see

---

\* Current affiliation: National Centers for Environmental Prediction Climate Prediction Center, Camp Springs, Maryland.

---

Corresponding author address: Dr. Hyun-kyung Kim, National Centers for Environmental Prediction/Climate Prediction Center, Rm. 605, 5200 Auth Rd., Camp Springs, MD 20746.  
E-mail: hyun-kyung.kim@noaa.gov

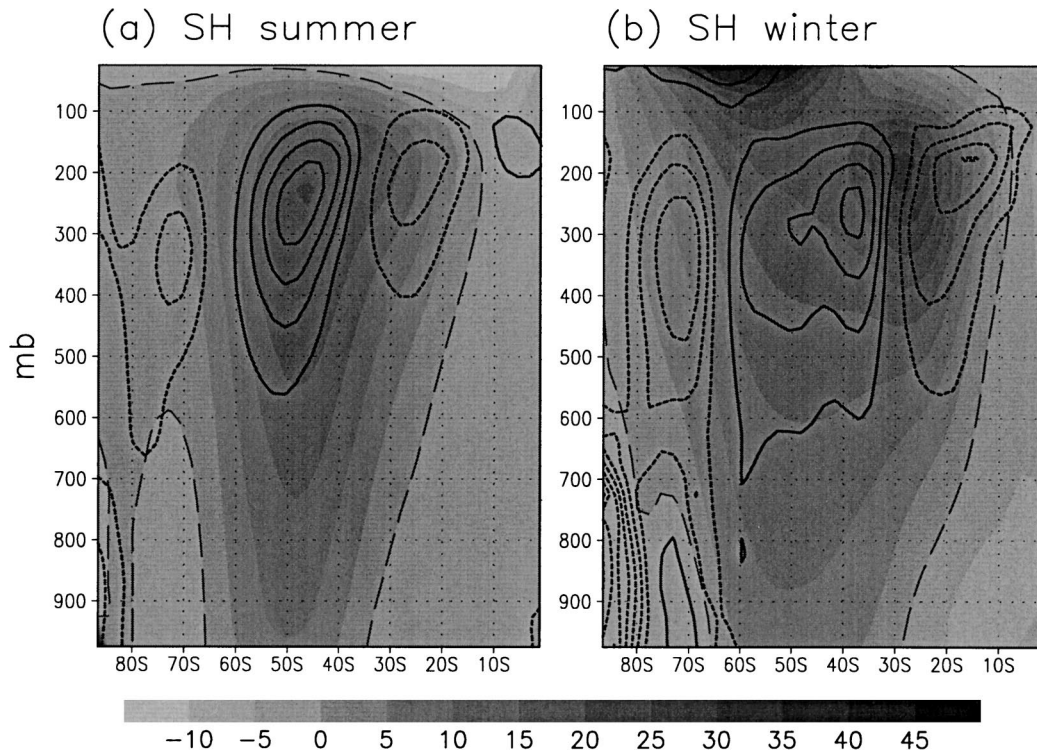


FIG. 1. The eddy momentum flux convergence (contours) superposed on the zonal mean zonal wind (shading) for the SH (a) summer and (b) winter. Contour interval is  $1 \times 10^{-5} \text{ m s}^{-2}$  and zero contours are omitted. Solid (dotted) contour lines represent the eddy momentum flux convergence (divergence). The shading scale is shown at the bottom of the figure. Dashed lines represent zero zonal mean zonal winds.

Fig. 1b), while there are hints of these two jets,<sup>1</sup> a subtropical jet at  $\sim 30^\circ\text{S}$  and a polar front jet at  $\sim 52^\circ\text{S}$ , this flow is clearly not characterized by two separate jets. The primary goal of this study is to investigate the reason why these two jets are not as well separated during the SH winter as one may expect. A useful clue is provided by the location of the maximum eddy momentum flux convergence; it lies *between* the two jets ( $\sim 40^\circ\text{S}$ ), not along the polar front jet ( $\sim 52^\circ\text{S}$ ). As such, most of this paper will focus on the nature of the disturbances

associated with this unusual eddy flux structure, and their possible role in merging the two jets.

The data and model used in this study are described in sections 2 and 3. Section 4 shows results from observational analyses, and motivates the eddy life cycle calculations presented in section 5. These calculations in turn prompt additional data analysis, and the results are shown in section 6. Section 7 describes results from numerical model experiments that are aimed at addressing the validity of the wave–zonal mean dynamical framework for the SH winter flow. The discussion and conclusions follow in section 8.

## 2. Data and diagnostic analysis

For this study, we use daily (0000 UTC) National Centers for Environmental Prediction–National Center for Atmospheric Research (NCEP–NCAR) reanalysis data extending from 1 January 1958 to 31 December 1997. The horizontal resolution is truncated at rhomboidal 30, and there are 28 unequally spaced sigma levels. To illustrate the results in pressure coordinates, logarithmic interpolation from sigma to pressure coordinates is performed.

Analyses are performed on the SH zonal mean zonal winds and on eddy momentum and heat fluxes. This

<sup>1</sup> The subtropical jet is identified by the top-heavy jet centered at  $30^\circ\text{S}$  and 200 mb, and the polar front (or eddy driven) jet can be discerned by a relatively deep structure near  $50^\circ\text{S}$ . Both jets can also be identified with the help of the surface winds. Axisymmetric circulation theory (Schneider 1977; Held and Hou 1980) predicts that the subtropical jet must be located at the poleward end of the Hadley cell; if the Coriolis torque is balanced by surface friction, which can be approximated as  $-\kappa u$ , where  $\kappa$  is a linear surface friction coefficient, it follows that the zonal wind at the surface at the poleward end of the Hadley cell, where  $v = 0$ , must also be zero. Figure 1b clearly shows a zero surface zonal wind at about  $30^\circ\text{S}$ . At the latitude of the eddy-driven jet, to maintain thermal wind balance, both the poleward eddy heat flux and the eddy momentum flux convergence drive a thermally indirect circulation (Phillips 1954). Again, if the Coriolis torque is to be balanced by the surface friction at the surface, then surface westerlies must develop. Thus, strong surface westerlies signify the eddy-driven jet. Figure 1b indeed shows the strongest surface westerlies near  $50^\circ\text{S}$ .

paper's main focus is the SH *winter* flow, because the subtropical and the polar front jets coexist during this season, and the degree of zonal inhomogeneity is less than that of the Northern Hemisphere (NH) winter flow. For comparison, however, some aspects of the SH summer flow are also presented. The SH summer and winter are defined as the periods from December through February (DJF), and from June through August (JJA), respectively.

### 3. Model description

The primitive equation (PE) model used in this paper is based on the dynamical core of the Geophysical Fluid Dynamics Laboratory (GFDL) general circulation model (e.g., Feldstein 1994; Kim and Lee 2001a,b). The horizontal resolution is truncated at rhomboidal 30, and there are 20 equally spaced sigma levels.

#### a. Inviscid eddy life cycle calculations

In addition to the forced-dissipative idealized model experiments to be described below, the above model is also used to perform "inviscid" eddy life cycle calculations. For these model calculations, there is no forcing and the flow is inviscid except for the inclusion of

quadarmonic ( $\nabla^4$ ) horizontal diffusion, which is used to represent the enstrophy cascade to subgrid scales. The coefficient for this horizontal diffusion is  $1 \times 10^{16} \text{ m}^4 \text{ s}^{-1}$ .

Two calculations are performed: one for the SH winter and the other for the SH summer. For each calculation, the model is initialized with the observed climatological flow. More specifically, given both the zonal mean temperature and the zonal mean surface pressure fields of the climatology, a nonlinearly balanced zonal wind field is obtained by using the secant method (e.g., Branscome et al. 1989; Feldstein 1994).

#### b. Model with empirical $T_E$ obtained by the "residual method"

The model is forced by thermal relaxation toward an empirical radiative-convective equilibrium temperature profile,  $T_E$ :

$$\frac{dT}{dt} \propto -\frac{T - T_E}{\tau},$$

where  $\tau$  is a relaxation time scale. This empirical  $T_E$  is obtained by adopting a "residual method" (James 1994) by utilizing the zonal mean, time mean thermodynamic energy equation in sigma coordinates:

$$[\bar{Q}] = \left[ \frac{\partial T}{\partial t} + \nabla \cdot (\mathbf{VT}) - T\nabla \cdot \mathbf{V} + \sigma \frac{\partial T}{\partial \sigma} - \frac{\kappa T \omega}{p_s \sigma} + K_h \nabla^8 T \right], \quad (1)$$

where  $[\cdot]$  denotes a zonal mean and  $\overline{(\cdot)}$  a time mean,  $\mathbf{V} = (u, v)$  is the horizontal wind vector,  $[\bar{Q}]$  is net observed diabatic heating, and  $\nabla$  is the gradient operator in

the latitude-longitude plane. After specifying  $[\bar{Q}] = -([\overline{T}] - T_E)/\tau$ , the "empirical"  $T_E$  profile takes the form of

$$T_E = \overline{[T]} - \tau \left[ -\nabla \cdot (\mathbf{VT}) + T\nabla \cdot \mathbf{V} - \sigma \frac{\partial T}{\partial \sigma} + \frac{\kappa T \omega}{p_s \sigma} - K_h \nabla^8 T - \frac{\partial T}{\partial t} \right]. \quad (2)$$

The notation is standard. Except for the relaxation time scale,  $\tau$ , all terms on the right-hand side of (2) can be obtained from the observational data. Note that the tendency term,  $[\partial T / \partial t]$ , is set to zero, as the averaging time period is regarded as sufficiently long. In essence, given that  $K_h$  is specified, the formulation (2) leaves us with  $\tau$  and the surface friction coefficient  $K_m$  [see (3)] in the momentum equation as the only free parameters in the model to be varied.

All of the dissipative processes, including surface friction and boundary layer processes, are parameterized by a linear damping:  $d\mathbf{V}/dt \propto -K_m \mathbf{V}$ . This simple representation allows us to readily examine the effect of

surface friction on statistically steady-state circulations. Following Held and Suarez (1994), the damping coefficient,  $K_m$ , takes the form of

$$K_m = \begin{cases} \frac{1}{\tau_m} \left( \frac{\sigma - \sigma_s}{1 - \sigma_s} \right) & \text{for } \sigma \geq \sigma_s, \\ 0 & \text{otherwise.} \end{cases} \quad (3)$$

The parameter  $\tau_m$  is the damping time scale, and  $\sigma_s$  is 0.7. The maximum value of  $K_m$  is applied at the surface, and  $K_m$  decreases with height. Above  $\sigma_s$ , the damping is set to zero. In this paper, the surface damping is described in terms of its time scale  $\tau_m$ .

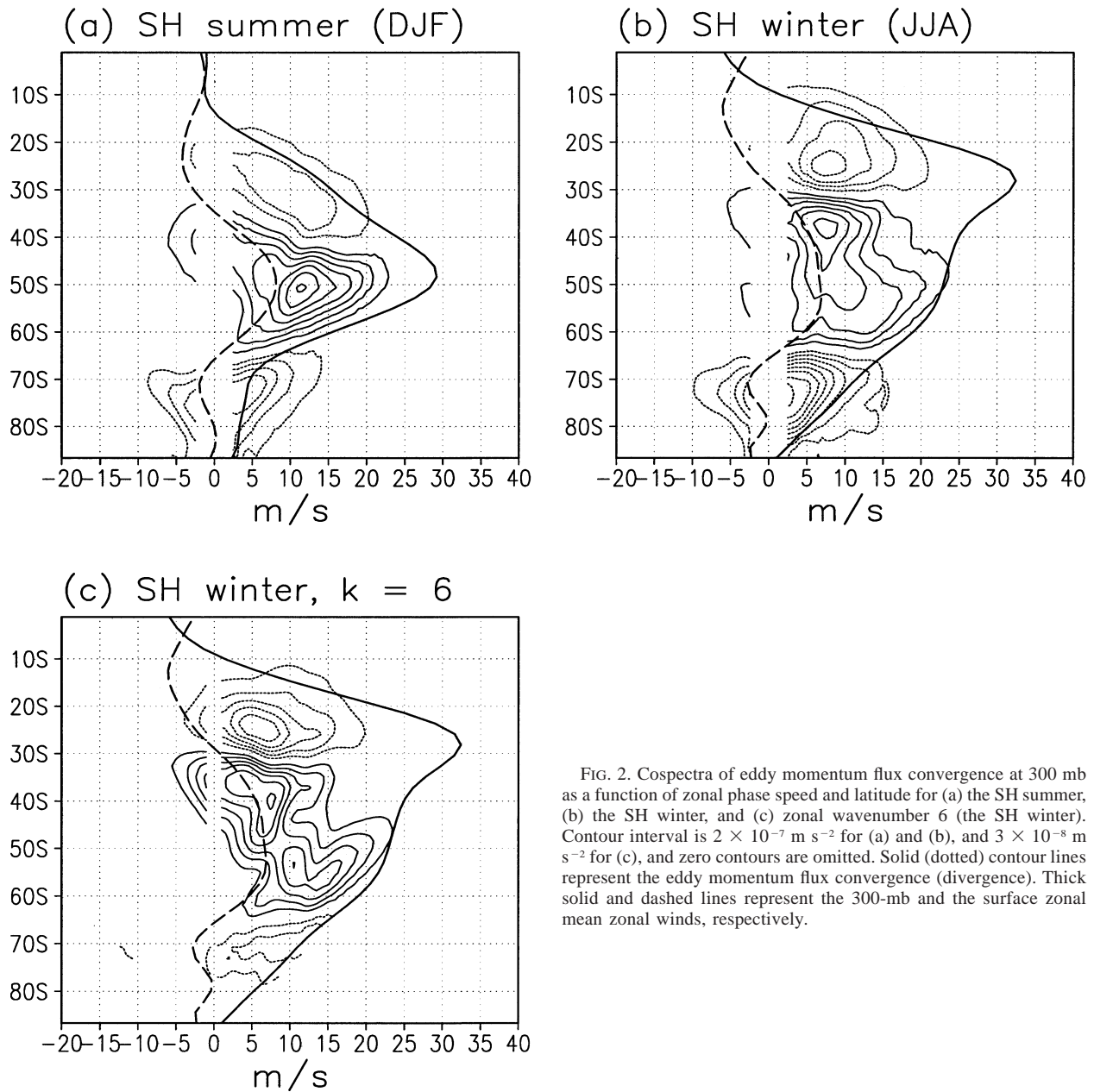


FIG. 2. Cospetra of eddy momentum flux convergence at 300 mb as a function of zonal phase speed and latitude for (a) the SH summer, (b) the SH winter, and (c) zonal wavenumber 6 (the SH winter). Contour interval is  $2 \times 10^{-7} \text{ m s}^{-2}$  for (a) and (b), and  $3 \times 10^{-8} \text{ m s}^{-2}$  for (c), and zero contours are omitted. Solid (dotted) contour lines represent the eddy momentum flux convergence (divergence). Thick solid and dashed lines represent the 300-mb and the surface zonal mean zonal winds, respectively.

The climatological zonal mean flow for the SH winter is used as an initial condition to obtain the statistically steady states for these model runs. Also, *zonal mean* topography is included at the surface to ensure that the initial climatological zonal mean flow is a balanced state.

#### 4. Cospetra of eddy fluxes

In order to characterize the disturbances that contribute to the zonal mean eddy fluxes, we examine cospetra of the eddy momentum flux convergence at 300 mb and eddy meridional heat flux at 700 mb, as a function of the zonal phase speed and latitude (Randel and Held

1991; Lee 1997). This analysis method is described by Hayashi (1971). For the purpose of comparison, both the SH summer and winter are examined. Figures 2a and 2b show cospetra of the eddy momentum flux convergence at 300 mb for the SH summer and winter, respectively. The area where the contours are discontinuous denotes the unresolved cosppectrum at low frequencies. To indicate the positions of the zonal mean jets, both the 300-mb and surface (994.5 mb) zonal mean zonal winds are displayed. Because the polar front jet is deeper than the subtropical jet (see Fig. 1b), the surface zonal wind is a better indicator of the polar front jet than the upper-tropospheric (300 mb) zonal wind.

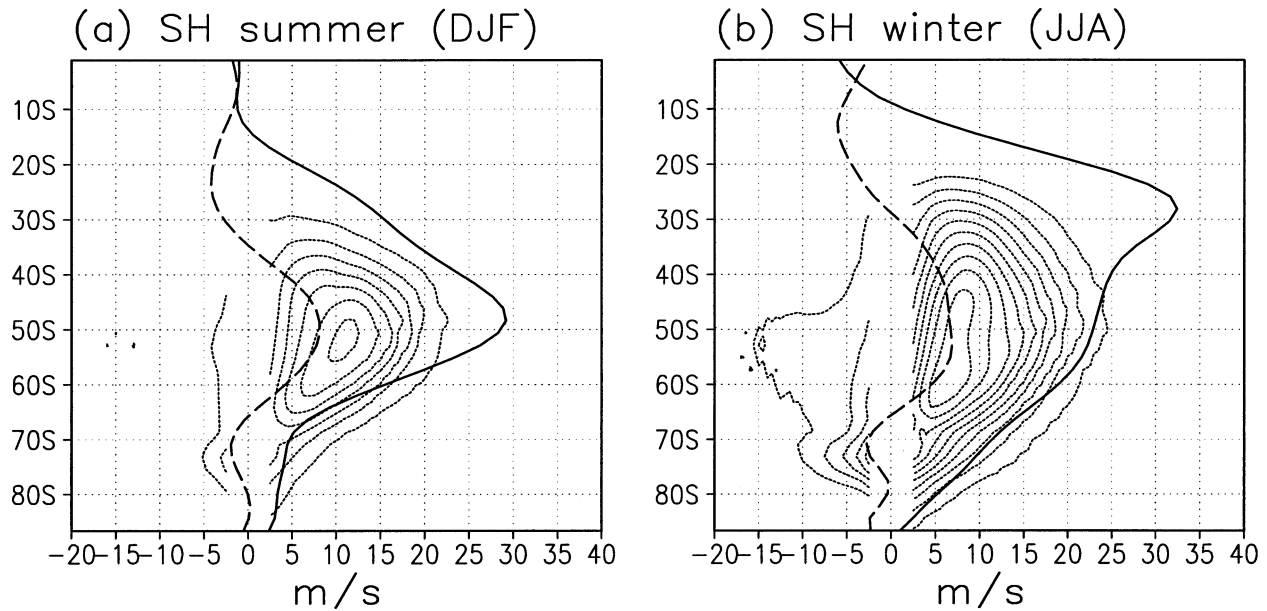


FIG. 3. As in Fig. 2 except for the eddy meridional heat flux at 700 mb for the SH (a) summer and (b) winter. Contour interval is  $0.05 \text{ K m s}^{-1}$  and zero contours are omitted. Solid (dotted) contour lines represent the equatorward (poleward) eddy meridional heat flux.

For the SH summer, consistent with the notion of an eddy-driven jet, the maximum eddy momentum flux convergence is found near the jet center (see contours in Fig. 2a). This momentum flux convergence is flanked by momentum flux divergence both in the subtropics and in high latitudes, indicating deceleration of the zonal mean zonal wind at those latitudes. As expected, the cospectrum of the eddy meridional heat flux at 700 mb shows a maximum poleward eddy meridional heat flux along the polar front jet (Fig. 3a).

For the SH winter, however, the cospectrum exhibits a more complex structure. Along the polar front jet, eddy momentum flux convergence still occurs. However, the maximum eddy momentum flux convergence occurs at  $\sim 37^\circ\text{S}$ , about halfway between the subtropical ( $\sim 28^\circ\text{S}$ ) and the polar front jets ( $\sim 52^\circ\text{S}$ ) (Fig. 2b). This feature can be seen more clearly if the cospectrum is plotted for individual zonal wavenumbers. For example, the cospectrum for zonal wavenumber 6 (Fig. 2c), the wave with the largest momentum flux convergence at  $40^\circ\text{S}$ , shows a clearer separation between two regions of eddy momentum flux convergence, one centered at  $40^\circ\text{S}$  with a phase speed  $c \approx 7.5 \text{ m s}^{-1}$  and the other centered at  $55^\circ\text{S}$  with  $c \approx 11 \text{ m s}^{-1}$ . The cospectrum of eddy meridional heat flux at 700 mb shows a latitudinally broad region of poleward eddy meridional heat flux (Fig. 3b), suggesting that the waves both at the polar front jet and between the two jets (see footnote 1) grow baroclinically.

To fix this idea, we refer to the baroclinic waves between the two jets, at  $\sim 40^\circ\text{S}$ , as interjet disturbances. This term, interjet disturbances (IJDs, hereafter), was first used in Lee (1997) to refer to baroclinically growing waves whose peak amplitude is located halfway between

two adjacent westerly jets. The suitability of this term for the case under consideration is discussed in section 8. For now, regardless of whether or not these SH winter disturbances can be identified as IJDs, it is fair to state that there seem to be important baroclinic disturbances that are not centered on the jets in the time mean flow. As such, the terminology of IJDs is used throughout this paper with this reservation in mind, and the focus of the rest of the study is to understand these rather unusual baroclinic disturbances and their role in altering the zonal mean flow.

## 5. Nonlinear eddy life cycles

In order to examine whether and how IJDs come into play during the course of the flow evolution, we first perform inviscid eddy life cycle calculations with the model described in section 3a. The initial state in these calculations corresponds to the zonal mean climatological flow. While this choice of initial flow may be objected to on the grounds that the climatological flow is already modified by the eddies, one may still ask how the eddies will evolve starting from “time averaged” flow conditions. The above initial flow is perturbed by a small-amplitude perturbation represented by the fastest-growing normal mode for zonal wavenumber 6. As can be inferred from the eddy heat and momentum flux structures during the first life cycle (see Figs. 4b, 5b, and 5c), these initial perturbations take on the well-known form (e.g., Simmons and Hoskins 1978, 1980) with their maximum amplitude coinciding with that of the polar front jet. Because the time that it takes for the unstable baroclinic waves to attain a finite amplitude depends upon the amplitude of the initial perturbation,

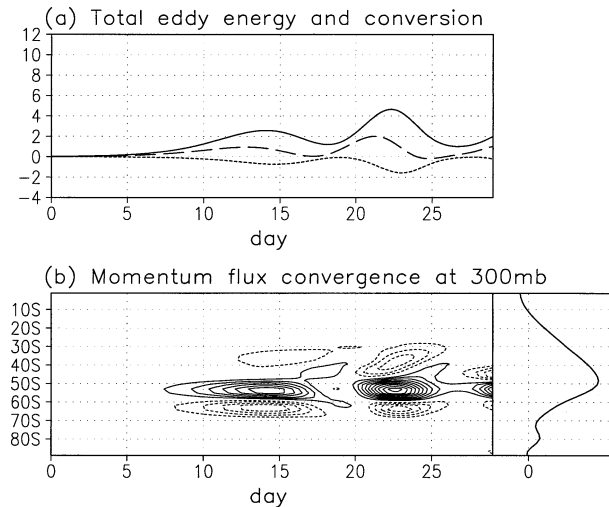


FIG. 4. Eddy life cycle calculation for the climatological SH summer initial state with zonal wavenumber 6. (a) Time evolution of the total eddy energy (solid line), the baroclinic energy conversion (dashed line), and the barotropic energy conversion (dotted line). The total eddy energy is normalized by  $1 \times 10^4 \text{ J m}^{-2}$ , and the energy conversion is normalized by  $1 \times 10^4 \text{ J m}^{-2} \text{ day}^{-1}$ . (b) Time evolution of the 300-mb eddy momentum flux convergence. Contour interval is  $3 \times 10^{-6} \text{ m s}^{-2}$  and zero contours are omitted. Solid (dotted) contours represent positive (negative) values. Right panel in (b) shows the zonal mean zonal wind at 300 mb averaged between 4 and 27 days.

we define day 0 to be the day that the growth rate starts to deviate from the linear growth rate.

#### a. SH summer initial state

To contrast the baroclinic wave evolution of the SH winter flow from that of the SH summer flow, we examine the latter case first. Figures 4a and 4b show the time evolution of the energetics and the eddy momentum flux convergence at 300 mb, respectively, for the SH summer initial state. In order to indicate the position of the jets, the time-averaged zonal mean zonal wind at 300 mb during the first two life cycles (between days 4 and 27) is displayed in the right panel of Fig. 4b. The energetic terms are calculated following Lorenz (1955), and the total eddy energy and energy conversions are integrated over the entire model atmosphere. There are several episodes of baroclinic growth and barotropic decay before the waves eventually decay altogether near day 100. Only the first two life cycles are displayed in Fig. 4a. The maximum eddy momentum flux convergence at 300 mb is located slightly poleward of the polar front jet, and is flanked by eddy momentum flux divergence at lower and higher latitudes. These baroclinic life cycles are very similar to those of previous studies in which the initial flow consists of one midlatitude jet (e.g., Simmons and Hoskins 1978; Branscome et al. 1989; Barnes and Young 1992; Feldstein 1994).

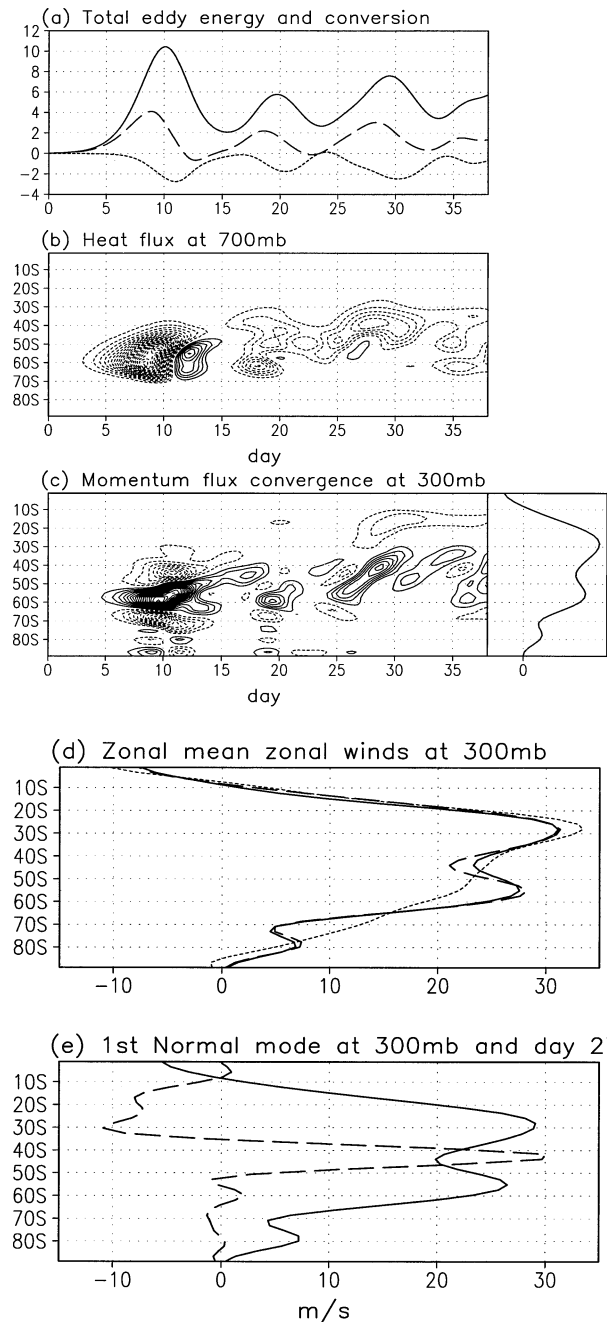


FIG. 5. Eddy life cycle calculation for the SH winter initial state with zonal wavenumber 6. (a) Time evolution of the total eddy energy (solid line), the baroclinic energy conversion (dashed line), and the barotropic energy conversion (dotted line). The total eddy energy is normalized by  $1 \times 10^4 \text{ J m}^{-2}$ , and the energy conversion is normalized by  $1 \times 10^4 \text{ J m}^{-2} \text{ day}^{-1}$ . Time evolution of (b) the 700-mb eddy heat flux and (c) the 300-mb eddy momentum flux convergence. Contour interval for (b) is  $0.5 \text{ K m s}^{-1}$  and for (c)  $3 \times 10^{-6} \text{ m s}^{-2}$ . Zero contours are omitted. Right panel in (c) shows the zonal mean zonal wind at 300 mb averaged between 4 and 27 days. (d) The 300-mb zonal mean zonal winds at day 25 (dashed line) and at day 35 (solid line). (e) The 300-mb eddy momentum flux convergence (dashed line) of the fastest-growing normal mode for the zonal mean flow at day 27 superposed on the 300-mb zonal mean zonal wind (solid line).

### b. SH winter initial state

For the SH winter initial state, Figs. 5a–c display the first three life cycles. The right panel in Fig. 5c shows the time-averaged zonal mean zonal wind at 300 mb during the first three life cycles (between days 3 and 33). During the first two life cycles, baroclinic waves grow and decay along the polar front jet. The baroclinic wave activity centered at  $\sim 58^\circ\text{S}$  accelerates the polar front jet and decelerates the zonal winds in the region between the subtropical and the polar front jets, and at higher latitudes (Fig. 5c). Note that the eddy momentum flux convergence associated with the first two initial life cycles does not invade the equatorward side of the subtropical jet.

The third life cycle, which emerges immediately after the gap between the two jets becomes sufficiently large (see the long-dashed curve in Fig. 5d), exhibits maximum eddy momentum flux convergence (divergence) at the interjet region (on the equatorward side of the subtropical jet). Consistent with the heat flux characteristics of IJDs (Lee 1997), during this third cycle, the maximum eddy heat flux peaks at the interjet region. It turns out that at the initial stage of this third cycle, the fastest-growing normal mode<sup>2</sup> of the zonal mean flow exhibits the SH winter IJD characteristics, with both the maximum poleward heat flux (not shown) and the maximum momentum flux convergence (dashed line in Fig. 5e) appearing at  $\sim 40^\circ\text{S}$ .

Although not shown, the main features of the third cycle are reproduced in a separate calculation in which the initial zonal flow is set equal to the zonal mean flow at day 27 in the integration shown in Fig. 5. In this calculation, the initial small-amplitude perturbation has the spatial structure of the fastest-growing normal mode (“IJD normal mode”) shown in Fig. 5e. This indicates that the emergence of the IJDs does not rely on multiple life cycles where the relevance of the latter life cycles, such as the third one in Fig. 5, is rather questionable.

We also performed another calculation to test if these IJDs can simply be interpreted as corresponding to secondary growth at the equatorward margin of the baroclinic zone, and not as a consequence of the presence of the two jets. In other words, we ask if a single-jet initial flow, provided that the baroclinicity is sufficiently strong, can still produce what we refer to as IJDs. To address this question, we perform a life cycle calculation in which the initial flow is obtained by modifying the SH summer flow. This initial flow is characterized by a single eddy-driven jet, as during the SH summer, yet the baroclinicity is specified to be greater than that of the SH summer flow so that the baroclinic eddies will saturate at a larger amplitude. This run produces multiple life cycles (not shown) with the maximum eddy

energy being comparable to that for the SH winter calculation. However, unlike for the IJD heat flux in the SH winter calculation (see the third cycle in Fig. 5b), in this new run, none of the life cycles exhibit poleward eddy heat fluxes whose maxima are at locations significantly far from the jet center (not shown).

While the significance of any single unstable normal mode and its idealized nonlinear life cycle needs to be taken with caution, these results suggest that the IJDs are preferentially excited when the jet separation is sufficiently distinct, and that the IJDs are an entity that can be clearly distinguished from the baroclinic waves that drive the polar front jet.

## 6. Observed temporal evolution of the baroclinic waves

The above eddy life cycle calculations assume that the relationship between the zonal mean flow and the eddies can be interpreted in the context of dynamics appropriate for a zonally homogeneous flow whose statistics are independent of longitude. While more zonally homogeneous than its Northern Hemisphere counterpart, the observed SH climatology does not satisfy the requirement of zonally homogeneous flow statistics. Thus, it is possible that the results of the above cospectra analyses are simply a zonal mean view of an inherently zonally asymmetric dynamical process, and that the agreement between the cospectra and the eddy life cycle calculations is fortuitous.

A definite proof of whether or not the *observed* IJDs can be framed in the context of wave–zonal mean flow interaction is extremely difficult. However, additional analyses and numerical experiments can be performed, which can either strengthen or weaken this possibility. For such a test, we perform composite analyses to examine if the transient evolution of the eddies in the atmosphere share qualitative similarities with the central results of the eddy life cycle calculations.

### a. Composite analyses based on momentum flux convergence

The composite criteria are based on the 300-mb zonal mean eddy momentum flux convergence both at  $53^\circ$  and  $37^\circ\text{S}$ . The former (latter) latitude corresponds to the location where the climatological eddy momentum flux convergence associated with the standard baroclinic waves (IJDs) reaches its maximum value. The data used are unfiltered, but the seasonal cycle is removed. Lag 0 corresponds to the day when the value of the zonal mean eddy momentum flux convergence reaches its maximum value, which must exceed 1.5 standard deviation. A negative (positive) lag indicates that the composite quantity leads (lags) the eddy momentum flux convergence at the reference latitude. A total of 108 and 112 cases are used for the composites based on the momentum flux convergence at  $53^\circ$  and  $37^\circ\text{S}$ , respec-

<sup>2</sup> The linearly unstable normal mode of the zonal mean flow at day 27 is calculated using a linearized version of the PE model described in section 3.

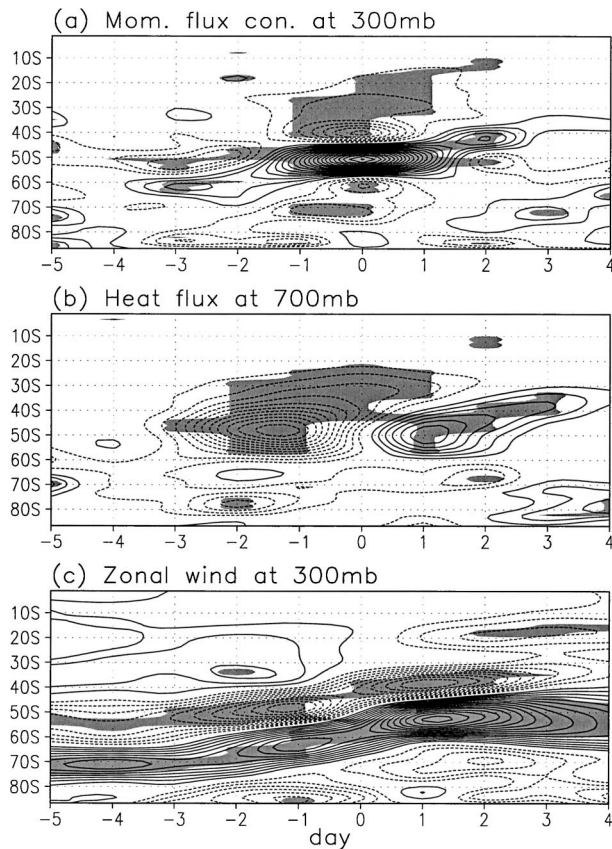


FIG. 6. Time-lagged composites of (a) zonal mean eddy momentum flux convergence at 300 mb, (b) zonal mean eddy meridional heat flux at 700 mb, and (c) zonal mean zonal wind anomaly at 300 mb, for large values of the maximum 300-mb zonal mean eddy momentum flux convergence at 53°S. Solid (dotted) contours denote positive (negative) values. Solid (dotted) contour lines in (c) represent westerly (easterly) zonal mean zonal wind anomalies. Contour interval is (a)  $5 \times 10^{-6} \text{ m s}^{-2}$ , (b)  $0.5 \text{ K m s}^{-1}$ , and (c)  $0.2 \text{ m s}^{-1}$ , and zero contours are omitted. Shaded values exceed the 95% confidence level of  $t$  values.

tively. The same qualitative results are found if linear regression is used instead (not shown).

The composites show that the observed temporal evolution of the baroclinic waves are, at least in a qualitative sense, broadly consistent with the results of the eddy life cycle calculations. Examining first the composites for the standard baroclinic waves, that is, with the base point at 53°S, the poleward heat flux leads the momentum flux convergence by about 1 day (cf. Figs. 6a and 6b), with the latitude of the maximum poleward eddy heat flux and maximum eddy momentum flux convergence consistent with those during the first life cycle (see the period between days 0 and 15 in Figs. 5b and 5c). This is followed by the strengthening of the polar front jet, and the weakening of the westerlies in the interjet region (Fig. 6c). Some of the more detailed points of agreement between the eddy life cycle calculations and these observational results include the equatorward heat flux anomaly near lag +1 day in Fig.

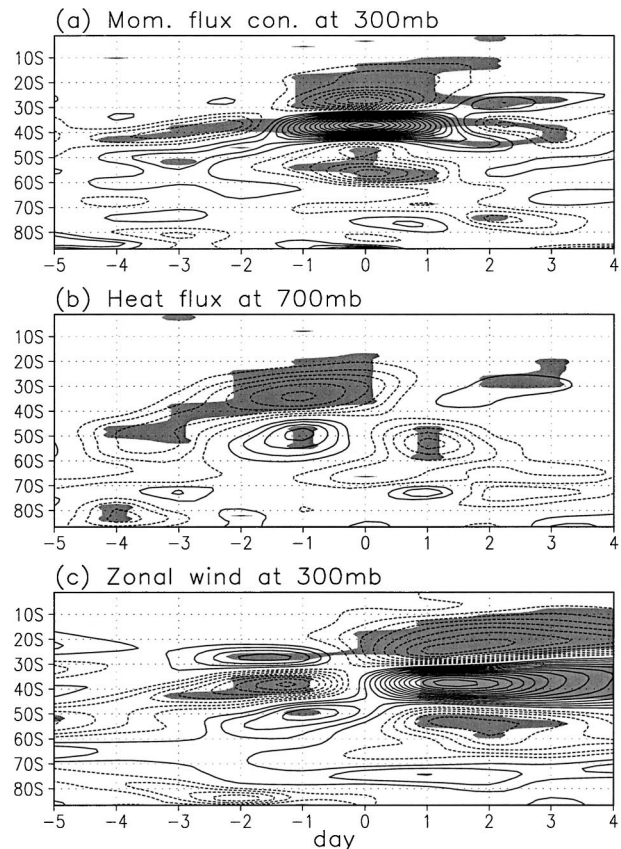


FIG. 7. As in Fig. 6 except for large values of the maximum 300-mb zonal mean eddy momentum flux convergence at 37°S.

6b and at day 12 in Fig. 5b, and the equatorward, with a hint of poleward, propagation of the momentum flux convergence between lag +1 and lag +2 days in Fig. 6a and at days 13–15 in Fig. 5c.

We next examine the temporal evolution of eddy fluxes for the eddy momentum flux convergence in the interjet region, that is, with a base point at 37°S. Again broadly consistent with the results of the life cycle calculation, the maximum eddy momentum flux convergence associated with the IJDs is preceded by eddy momentum flux convergence at the latitude of the polar front jet (see Fig. 7a), and a pronounced separation between the subtropical and the polar front jets (see lag -1 in Fig. 7c). Furthermore, significant momentum flux divergence can be seen between 30° and 10°S, on the equatorward side of the subtropical jet. Note that the momentum flux *divergence* associated with the standard baroclinic waves peaks at the latitudes where the IJD momentum flux *convergence* takes place, not on the equatorward side of the subtropical jet. The property that the poleward eddy meridional heat flux at 700 mb propagates from the latitude of the polar front jet to the latitude of the IJDs (from lag -4 to lag -2 days in Fig. 7b), and that it leads the momentum flux convergence by 1–2 days, also compares reasonably well with its life

cycle counterpart (cf. Figs. 5b and 7b). In the life cycle calculation at day 27 (Fig. 5b), there is a weak equatorward eddy heat flux to the south of the major poleward heat flux associated with IJDs. The same general pattern can be found in Fig. 7b. All of these features support that IJDs are not simply part of standard baroclinic waves.

### b. Composite analyses based on the SH zonal index

Taking the above composite analysis one step further, we show that the IJDs play a central role for the SH winter zonal index (Hartmann and Lo 1998; Feldstein 2000). We define the zonal index (ZI) as the principal component of the first empirical orthogonal function (EOF) of the daily zonal mean zonal wind at the 300-mb level. This first EOF explains 29% of total variance and represents fluctuations between double-jet and single-jet states. This spatial pattern is very similar to Fig. 4 in Hartmann and Lo (1998) and Fig. 2 in Feldstein (2000), and can be inferred from Figs. 8b and 8c in this paper. The positive phase of the ZI corresponds to the double-jet state, and the negative phase to the single-jet state.

In order to investigate the possible role of the IJDs in the transition from the positive to the negative phase of the ZI, we perform a composite analysis based on both the ZI and its tendency. First, the absolute value of the ZI tendency must be greater than one standard deviation. Second, lag 0 corresponds to the day when the absolute value of the tendency reaches the local maximum, and the value of the ZI changes sign from positive to negative. A total of 80 cases are used for the composite analyses.

The main features of the resulting composites (Fig. 8) share unmistakable similarities with those shown in Fig. 7. At lag  $-2$  days, there is an enhanced momentum flux convergence (Fig. 8a) at the latitude of the polar front jet. At this time, the zonal wind anomaly (Fig. 8b) shows a clear sign of reduced westerlies centered at  $40^{\circ}\text{S}$ . Two days later, we observe an emergence of momentum flux convergence maximum at this same latitude, along with the corresponding momentum flux divergence in the lower latitudes. Although not shown, as with Fig. 7b, the poleward eddy heat flux peaks 1 day earlier, again at  $40^{\circ}\text{S}$ . These heat and momentum flux characteristics are consistent with the IJDs seen in Figs. 5 and 7. The total zonal mean flow, shown in Fig. 8c, clearly demonstrates the transition from the double-jet state of the positive ZI phase to the single-jet state of the negative ZI phase. We thus conclude that the IJDs play an important role for the SH winter ZI, and that the result shown in Fig. 7 is not the consequence of a contrived choice of the base latitude.

## 7. Numerical experiments

We examine whether interjet disturbances similar to those observed during the SH winter can be found in a

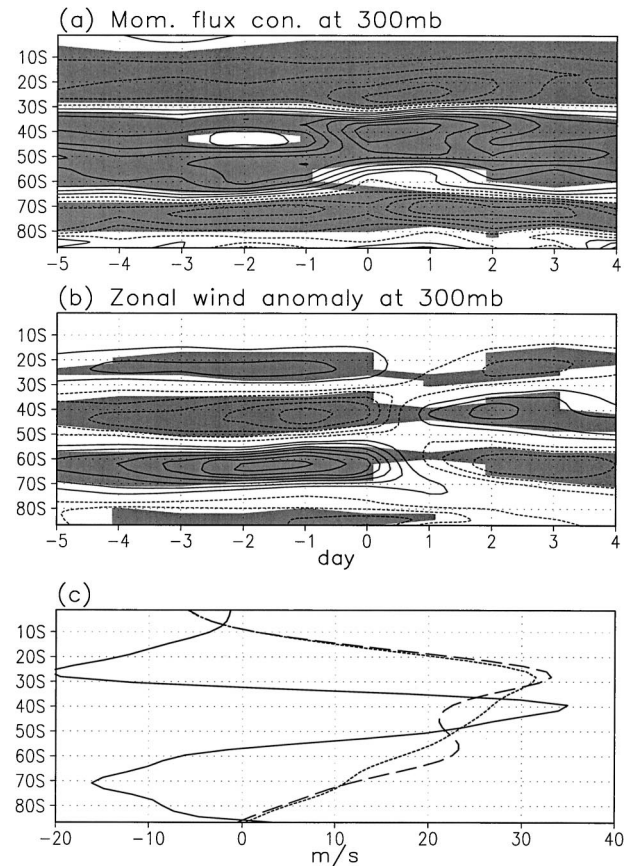


FIG. 8. Time-lagged composites of (a) zonal mean eddy momentum flux convergence at 300 mb, and (b) zonal mean zonal wind anomaly at 300 mb based on both the ZI and its tendency. Solid (dotted) contours denote positive (negative) values. Solid (dotted) contour lines in (b) represent westerly (easterly) zonal mean zonal wind anomalies. (c) The 300-mb eddy momentum flux convergence (solid line) at lag 0 superimposed on the 300-mb zonal mean zonal wind at lag  $-1$  days (dashed line) and at lag  $+2$  days (dotted line). The contour interval in (a) is  $1 \times 10^{-5} \text{ m s}^{-2}$ , in (b) it is  $0.5 \text{ m s}^{-1}$ , and the zero contour is omitted. Shaded values exceed the 95% confidence level of  $t$  values.

flow with zonally homogeneous statistics. To address this question, we perform a forced-dissipated run with the same PE model used earlier in this study. For these calculations, the model temperature is relaxed toward a zonally uniform, empirical  $T_E$  profile obtained from (2) for the SH winter, with  $\tau = 20$  days (see Fig. 9).

Driven by the empirical  $T_E$  profile, the PE model is integrated until a statistically steady state is reached. Figure 10 shows the eddy momentum flux convergence superimposed upon the zonal mean zonal wind for the statistically steady state with a surface damping time scale  $\tau_m$  set to 1 day. The statistically steady state is obtained from the last 1500 days of the 1800-day-long integration. While the PE model includes only simple physics and zonally symmetric surface boundary conditions and forcing, the structure of both the zonal mean zonal wind and that of the eddy momentum flux con-

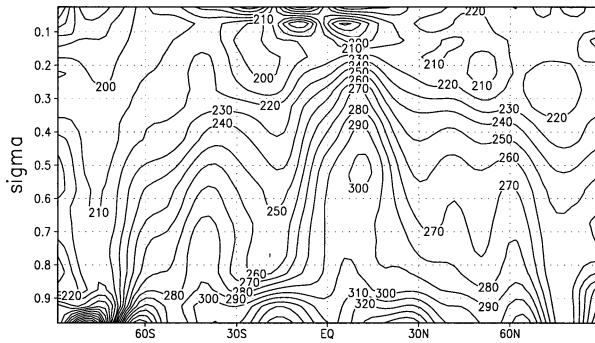


FIG. 9. The empirical profile for  $T_E$  is obtained from observations with  $\tau = 20$  days. The contour interval is 10 K.

vergence are very similar to their observed counterparts (cf. Fig. 10 with Fig. 1b).

The spectral characteristics of the interjet disturbances are also well represented in this model. Figure 11 shows the cospectrum of the eddy momentum flux convergence at 325 mb as a function of zonal phase speed and latitude. Similar to observations (see Fig. 2b), one eddy momentum flux convergence maximum occurs between the two jets near 38°S (i.e., interjet disturbances) and another occurs near 50°S at the polar front jet.

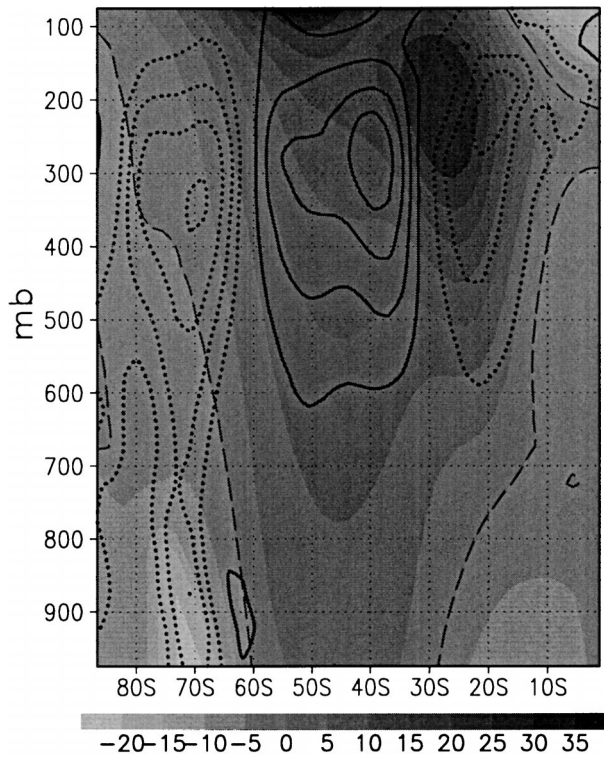


FIG. 10. The eddy momentum flux convergence (contours) superposed on the zonal mean zonal wind (shading) from the statistically steady state with the empirical  $T_E$  profile obtained from observations. The contour interval is  $1 \times 10^{-5} \text{ m s}^{-2}$ , and zero contours are omitted. The shading scale is shown at the bottom of the figure and dashed lines represent the zero zonal mean zonal wind value. The shading interval is  $5 \text{ m s}^{-1}$ .

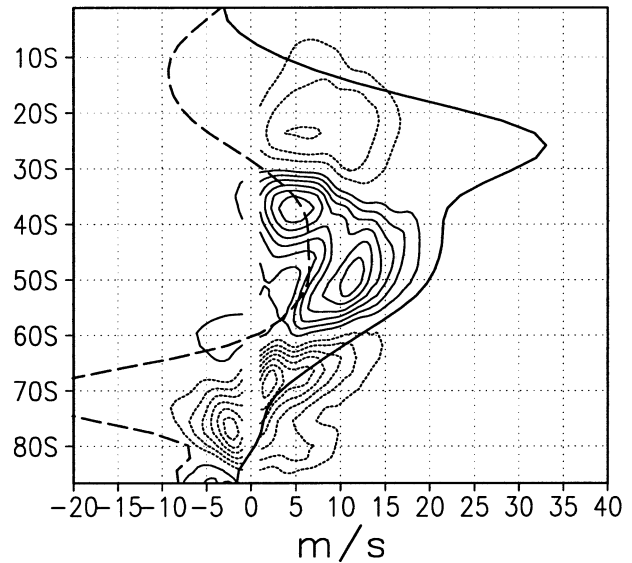


FIG. 11. As in Fig. 2b except for the statistically steady state with the empirical  $T_E$  profile. Thick solid and dashed lines represent the 325-mb and surface zonal mean zonal winds, respectively. The contour interval is  $3 \times 10^{-7} \text{ m s}^{-2}$ , and zero contours are omitted.

Because  $\tau_m$  is a free parameter of this model, we briefly discuss the sensitivity of the above results to the value of  $\tau_m$ . Figure 12 shows the latitude of the polar front jet with various values of  $\tau_m$  (0.5, 1, 2, 3, and 4 days). Previous studies of idealized general circulation models with simple physics show that the polar front jet shifts equatorward as surface friction increases (James and Gray 1986; Robinson 1997). Consistent with these earlier results, when  $\tau_m$  decreases from 4 to 2 days (i.e., the surface friction increases), the polar front jet moves equatorward. When  $\tau_m$  is further reduced to 1 day, however, the polar front jet moves poleward to  $\sim 48^\circ\text{S}$ . Currently, we do not have an explanation for this behavior. Despite this sensitivity, for four of five

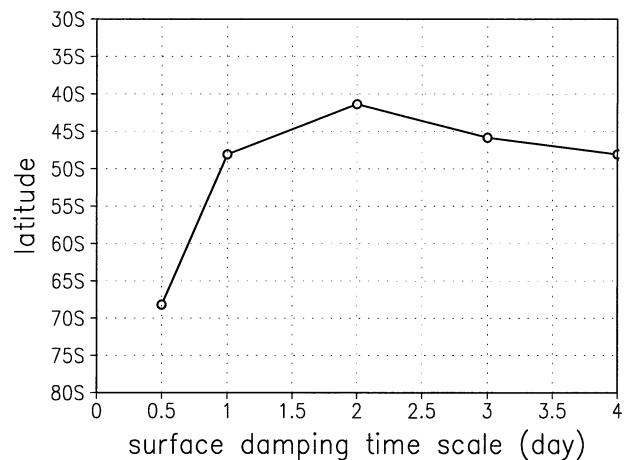


FIG. 12. The latitude of the polar front jet for various surface damping time scales.

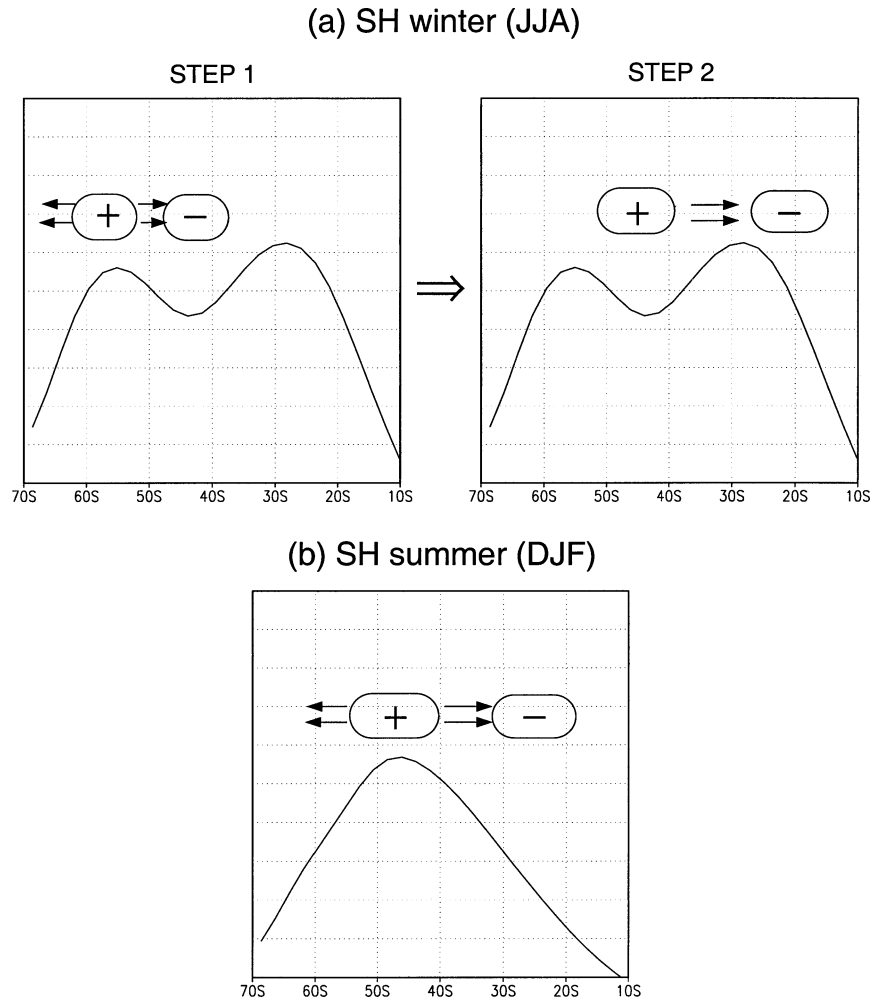


FIG. 13. A schematic diagram of baroclinic wave activity in the upper troposphere for the SH (a) winter and (b) summer. A plus (minus) sign indicates eddy momentum flux convergence (divergence) and arrows indicate the direction of wave activity flux (opposite direction to that of the eddy momentum flux). The solid curve indicates the upper-tropospheric zonal mean zonal wind. In the upper-right panel, the zonal mean zonal wind response to the IJD momentum flux is indicated by a thick-dashed curve.

cases ( $\tau_m = 1, 2, 3,$  and  $4$  days) described above, the eddy momentum flux convergence maximum is always found between the subtropical and polar front jets (not shown). Discussion of the case with  $\tau_m = 0.5$  is deferred to section 8.

## 8. Discussion and concluding remarks

In this paper, we investigate the maintenance mechanisms of the climatological zonal mean zonal winds during the SH winter, focusing on the role of baroclinic waves. The SH winter is chosen because 1) the flow is more zonally symmetric than the NH winter flow, allowing for a simpler dynamical interpretation, and (2) the subtropical jet is prominent during the winter season.

The results of this study suggest that the presence of rather unusual baroclinic waves, which we refer to as

interjet disturbances (IJDs), helps to explain the rather complex eddy momentum and zonal wind structure in the SH winter zonal flow. The presence of the so-called IJDs in the SH winter flow is suggested by the following results.

- The cospectrum, especially for zonal wavenumber 6 (see Fig. 2c), shows two centers of eddy momentum flux convergence with distinct phase speeds, one along the polar front jet and the other in the interjet region.
- In the baroclinic life cycle, the growth of the IJDs is associated with a “cycle” of growth and decay that is separate from that of the standard baroclinic waves.
- The qualitative behavior of the eddy fluxes in the life cycle calculations holds for its observed counterpart.
- While the relevance of a single normal mode should be taken with caution, in the life cycle calculations,

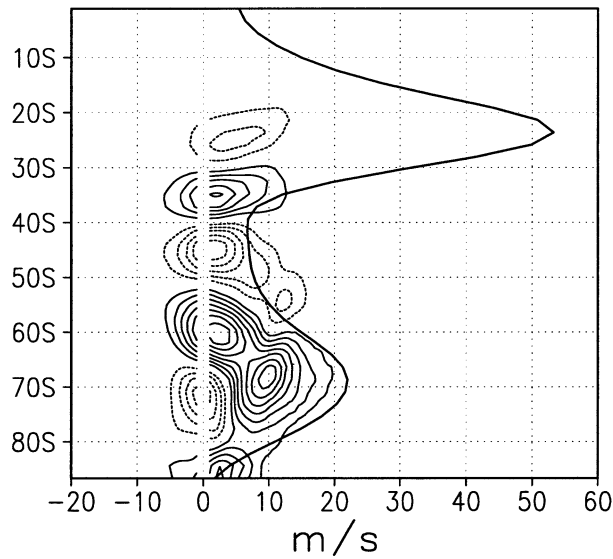


FIG. 14. As in Fig. 11 except for  $\tau_m = 0.5$  day. The contour interval is  $2 \times 10^{-7} \text{ m s}^{-2}$ , and zero contours are omitted.

a short time prior to the IJD growth when the distinction between the polar front and subtropical jets becomes clear, the most unstable normal mode of the flow turns out to be the IJD mode (Fig. 5e).

- Numerical experiments show that as surface friction increases, the IJD momentum flux changes sign (cf. Figs. 11 and 14). As a result, for a sufficiently strong surface friction, the IJD momentum flux diverges in the interjet region, resulting in a separation of the two jets (see Fig. 14). This result not only exemplifies the sensitivity of the eddy momentum flux structure in a baroclinically unstable flow (Held 1975), but also supports the view that the unusual baroclinic disturbances in the SH winter can indeed be regarded as IJDs in the sense of Lee (1997). Clearly, a more careful study is called for in order to better understand the IJDs, and their relevance for the SH winter flow.

The results from both the eddy life cycle calculations and the composite analyses are summarized in Fig. 13a, which depicts a schematic diagram of the eddy momentum flux convergence in the upper troposphere together with the two jets. Baroclinic waves are first excited and grow at the latitude of the polar front jet. Subsequent barotropic decay of the eddies accompanies an acceleration of the polar front jet and a deceleration of the westerly zonal winds between the two jets (step 1). Once these two distinct jets are well established, then the IJDs start to grow between the two jets (step 2). As these IJDs propagate equatorward, they accelerate (decelerate) the westerly zonal winds between the two jets (on the equatorward side of the subtropical jet). For comparison, Fig. 13b shows an analogous schematic diagram for the SH summer eddy life cycle that bears a close resemblance to those reported in previous studies

(e.g., Simmons and Hoskins 1978, 1980; Edmon et al. 1980; Hoskins 1983; Held and Hoskins 1985, etc.).

When the model is driven by an equilibrium temperature profile derived from observations, the characteristics of the IJDs are successfully simulated. Since the model has *zonally symmetric* surface boundary conditions, these results support the use of the *zonal mean dynamical* framework.

As has been demonstrated by previous studies (e.g., Suarez and Duffy 1992; Saravanan 1993), the structure of the eddy momentum flux is rather sensitive to the external forcing. These studies also underscore the fact that the eddy momentum flux plays a key role in determining the structure of the general circulation. To highlight this point in the context of the present work, we reconsider the numerical experiments discussed in section 7. Referring back to Fig. 12, a change in the position of the polar front jet occurs when  $\tau_m$  decreases from 1 to 0.5 days. For  $\tau_m = 0.5$  days, the polar front jet is found at a latitude of  $\sim 68^\circ\text{S}$ , much farther poleward than that for the  $\tau_m = 1$  day case (see Fig. 14). This substantial circulation change is consistent with a sign change in the IJD momentum flux convergence; unlike for all other cases, for  $\tau_m = 0.5$  day, the IJD momentum flux *diverges* between the two jets, *maintaining* a two-jet state as in Lee (1997). These results not only support the IJDs as a separate entity, but also suggest that the IJDs can play a crucial role in determining even the qualitative structure of the SH winter circulation.

Finally, even if one accepts the existence of IJDs, a fundamental question still remains as to why the peak baroclinic wave activity takes place in the zonal wind minimum, and not along the wings of the jet. We suspect that the so-called barotropic governor mechanism (James 1987; James and Gray 1986; Nakamura 1993) is at least partially responsible for this feature. Nakamura shows that as barotropic shear increases, the meridional scale of baroclinic modes decreases, diminishing their ability to tap available potential energy. The relevance of this mechanism for the existence of IJDs can certainly be tested, but this is beyond the scope of this study.

*Acknowledgments.* We would like to thank Dr. Steven Feldstein for providing us with the computer code that was used to obtain the nonlinearly balanced states. His comments on this manuscript are also appreciated. The NCEP–NCAR reanalysis data were provided by the Climate Diagnostic Center. This research was supported by the National Science Foundation through Grant ATM-0001473.

## REFERENCES

- Andrews, D. G., and M. E. McIntyre, 1976: Planetary waves in horizontal and vertical shear: The generalized Eliassen–Palm re-

- lation and the mean zonal acceleration. *J. Atmos. Sci.*, **33**, 2031–2048.
- , and —, 1978: Generalized Eliassen–Palm and Charney–Dragon theorems for waves on asymmetric mean flows in compressible atmospheres. *J. Atmos. Sci.*, **35**, 175–185.
- Barnes, J. R., and R. E. Young, 1992: Nonlinear baroclinic instability on the sphere: Multiple life cycle with surface drag and thermal damping. *J. Atmos. Sci.*, **49**, 861–878.
- Branscome, L. E., W. J. Gutowski Jr., and D. A. Stewart, 1989: Effect of surface fluxes on the nonlinear development of baroclinic waves. *J. Atmos. Sci.*, **46**, 460–475.
- Edmon, H. J., B. J. Hoskins, and M. E. McIntyre, 1980: Eliassen–Palm cross sections for the troposphere. *J. Atmos. Sci.*, **37**, 2600–2616.
- Eliassen, A., and E. Palm, 1961: On the transfer of energy in stationary mountain waves. *Geophys. Publ.*, **22** (3), 1–23.
- Feldstein, S. B., 1994: A weakly nonlinear primitive equation baroclinic life cycle. *J. Atmos. Sci.*, **51**, 23–34.
- , 2000: The timescale, power spectra, and climate noise properties of teleconnection patterns. *J. Climate*, **13**, 4430–4440.
- , and I. M. Held, 1989: Barotropic decay of baroclinic waves in a two-layer beta-plane model. *J. Atmos. Sci.*, **46**, 3416–3430.
- Hartmann, D. L., and F. Lo, 1998: Wave-driven zonal flow vacillation in the Southern Hemisphere. *J. Atmos. Sci.*, **55**, 1303–1315.
- Hayashi, Y., 1971: A generalized method of resolving disturbances into progressive and retrogressive waves by space Fourier and time cross-spectral analyses. *J. Meteor. Soc. Japan*, **49**, 125–128.
- Held, I. M., 1975: Momentum transport by quasi-geostrophic eddies. *J. Atmos. Sci.*, **32**, 1494–1497.
- , and A. Y. Hou, 1980: Nonlinear axially symmetric circulations in a nearly inviscid atmosphere. *J. Atmos. Sci.*, **37**, 515–533.
- , and B. J. Hoskins, 1985: Large-scale eddies and the general circulation of the troposphere. *Advances in Geophysics*, Vol. 28A, Academic Press, 3–31.
- , and M. J. Suarez, 1994: A proposal for the intercomparison of the dynamical cores of atmospheric general circulation models. *Bull. Amer. Meteor. Soc.*, **75**, 1825–1830.
- Holopainen, E. O., 1978: On the dynamic forcing of the long-term mean flow by the large-scale Reynolds' stresses in the atmosphere. *J. Atmos. Sci.*, **35**, 1596–1604.
- Hoskins, B. J., 1983: Modelling of the transient eddies and their feedback on the mean flow. *Large-Scale Dynamical Processes in the Atmosphere*, B. J. Hoskins and R. P. Pearce, Eds., Academic Press, 169–199.
- James, I. N., 1987: Suppression of baroclinic instability in horizontally sheared flows. *J. Atmos. Sci.*, **44**, 3710–3720.
- , 1994: *Introduction to Circulating Atmospheres*. Cambridge University Press, 422 pp.
- , and L. J. Gray, 1986: Concerning the effect of surface drag on the circulation of a baroclinic planetary atmosphere. *Quart. J. Roy. Meteor. Soc.*, **112**, 1231–1250.
- Kim, H., and S. Lee, 2001a: Hadley cell dynamics in a primitive equation model. Part I: Axisymmetric flow. *J. Atmos. Sci.*, **58**, 2845–2858.
- , and —, 2001b: Hadley cell dynamics in a primitive equation model. Part II: Nonaxisymmetric flow. *J. Atmos. Sci.*, **58**, 2859–2871.
- Kuo, H.-L., 1953: On the production of mean zonal currents in the atmosphere by large disturbances. *Tellus*, **5**, 475–493.
- Lee, S., 1997: Maintenance of multiple jets in a barocline flow. *J. Atmos. Sci.*, **54**, 1726–1738.
- , and H. Kim, 2003: The dynamical relationship between subtropical and eddy-driven jets. *J. Atmos. Sci.*, **60**, 1490–1503.
- Lorenz, E. N., 1955: Available potential energy and the maintenance of the general circulations. *Tellus*, **7**, 157–167.
- Nakamura, N., 1993: Momentum flux, flow symmetry, and the nonlinear barotropic governor. *J. Atmos. Sci.*, **50**, 2159–2179.
- Palmén, E., and C. W. Newton, 1969: *Atmospheric Circulation Systems*. Academic Press, 603 pp.
- Phillips, N. A., 1954: Energy transformations and meridional circulation associated with simple baroclinic waves in a two-level, quasi-geostrophic model. *Tellus*, **6**, 273–286.
- Randel, W. J., and I. M. Held, 1991: Phase speed spectra of transient eddy fluxes and critical layer absorption. *J. Atmos. Sci.*, **48**, 688–697.
- Robinson, W. A., 1997: Dissipation dependence of the jet latitude. *J. Climate*, **10**, 176–182.
- Saravanan, R., 1993: Equatorial superrotation and maintenance of the general circulation in two-level models. *J. Atmos. Sci.*, **50**, 1211–1227.
- Schneider, E. K., 1977: Axially symmetric steady-state models of the basic state for instability and climate studies. Part II. Nonlinear calculations. *J. Atmos. Sci.*, **34**, 280–297.
- Simmons, A. J., and B. J. Hoskins, 1978: The life cycles of some nonlinear baroclinic waves. *J. Atmos. Sci.*, **35**, 414–432.
- , and —, 1980: Barotropic influences on the growth and decay of nonlinear baroclinic waves. *J. Atmos. Sci.*, **37**, 1679–1684.
- Starr, V. P., 1953: Note concerning the nature of the large-scale eddies in the atmosphere. *Tellus*, **5**, 494–498.
- Suarez, M. J., and D. G. Duffy, 1992: Terrestrial superrotation: A bifurcation of the general circulation. *J. Atmos. Sci.*, **49**, 256–269.
- Thompson, R., 1980: A prograde jet driven by Rossby waves. *J. Atmos. Sci.*, **37**, 1216–1226.